

This document is confidential and is proprietary to the American Chemical Society and its authors. Do not copy or disclose without written permission. If you have received this item in error, notify the sender and delete all copies.

The Effect of Ageing and PCBM content on Bulk Heterojunction Organic Solar Cells Studied by Intensity Modulated Photocurrent Spectroscopy

Journal:	<i>ACS Applied Materials & Interfaces</i>
Manuscript ID	am-2016-03892n.R1
Manuscript Type:	Article
Date Submitted by the Author:	n/a
Complete List of Authors:	Byers, Joshua; The University of Western Ontario, Department of Chemistry Heiser, Thomas; InESS, Skorobogatiy, Maksim; Ecole polytechnique de Montreal, Department of Engineering physics Semenikhin, Oleg; The University of Western Ontario, Department of Chemistry

SCHOLARONE™
Manuscripts

1
2
3
4
5
6
7 The Effect of Ageing and PCBM content on Bulk
8
9
10
11 Heterojunction Organic Solar Cells Studied by
12
13
14
15 Intensity Modulated Photocurrent Spectroscopy
16
17
18
19
20

21 *Joshua C. Byers,^{†Δ} Thomas Heiser,[‡] Maksim Skorobogatiy,[§] Oleg A. Semnikhin^{*†}*
22
23

24 † Department of Chemistry, The University of Western Ontario, 1151 Richmond St., London,
25
26 Ontario, N6A 5B7, Canada
27
28

29
30 ‡ Institut d'Electronique du Solide et des Systèmes, Université de Strasbourg-CNRS, 23 rue du
31
32 Loess, 67037 Strasbourg, France
33
34

35
36 § Génie Physique, École Polytechnique de Montréal, C.P. 6079, succ. Centre-ville, Montréal,
37
38 Québec, H3C 3A7, Canada
39
40
41
42
43
44
45
46
47

48 **Keywords.** Organic photovoltaics, intensity modulated photocurrent spectroscopy (IMPS),
49
50 intensity modulated photovoltage spectroscopy (IMVS), exciton, degradation, non-geminate
51
52 recombination.
53
54
55
56
57
58
59
60

1
2
3
4 **Abstract.** A series of encapsulated and non-encapsulated bulk heterojunction photovoltaic
5 devices containing poly(3-hexylthiophene) (P3HT) and [6,6]-phenyl C₆₁ butyric acid methyl
6 ester (PCBM) with different P3HT:PCBM ratios were investigated using traditional steady state
7 as well as non-steady state intensity modulated photocurrent spectroscopy (IMPS) techniques.
8
9 The steady state J-V measurements showed that PCBM content did not have a significant effect
10 on the efficiency for freshly prepared devices, whereas aged non-encapsulated devices exhibited
11 a strong dependence on PCBM content. IMPS measurements showed a significant contribution
12 of interfacial non-geminate recombination in non-encapsulated devices, which increased with
13 decreasing PCBM content in the photoactive layer and cell aging. It was related to the formation
14 of interfacial states at the P3HT/PCBM interface due to atmospheric contamination, which act as
15 recombination centers. Device encapsulation was found to be effective in preventing the
16 occurrence of interfacial recombination. Our results suggest that IMPS can be used as a
17 diagnostic tool to predict the performance of bulk heterojunction organic solar cells. If a solar
18 cell shows the presence of interfacial states as indicated by semicircle arcs in quadrant I of the
19 IMPS complex plane plots, it is most likely that its performance will deteriorate with time due to
20 enhanced interfacial recombination, even without further exposure to atmospheric
21 contaminations. We conclude that interfacial non-geminate recombination is an important
22 degradation mechanism in organic solar cells, especially in case of exposure to atmospheric
23 contaminants.
24
25
26
27
28
29
30
31
32
33
34
35
36
37
38
39
40
41
42
43
44
45
46
47
48
49
50
51
52
53
54
55
56
57
58
59
60

1. Introduction

Bulk heterojunction organic solar cells incorporating conjugated polymers and fullerene derivatives as a composite photoactive layer represent a promising platform for high-throughput, low cost alternative energy generation. Organic photovoltaic devices require the use of two materials in the photoactive layer due to the formation of excitons, instead of free charge carriers, upon light absorption in the conjugated polymer. Due to the short lifetimes of excitons, it is necessary to form an intimately mixed three dimensional bulk heterojunction of the two materials to maximize the interfacial area while ensuring the formation of uninterrupted pathways for charge carriers to be transported across the film. However, even then, a significant fraction of photogenerated carriers is lost due to recombination. Generally, two recombination mechanisms are considered: geminate recombination whereby both recombining carriers are generated simultaneously and form a primary exciton, and non-geminate recombination, which involves an electron and a hole that were photogenerated in separate acts and possibly quite far from each other. In the latter case, the recombination is often assisted by interfacial states, which can be envisioned as local states or traps that are located at an interface between two phases (e.g., PCBM and P3HT or PCMB or P3HT and metal contact, etc) and can be accessed both by photogenerated electrons or holes. In recent years, non-geminate recombination has emerged as an important pathway of recombination losses in organic bulk heterojunction solar cells.¹⁻³ However, the mechanism of the recombination process and especially the origin of the interfacial states where non-geminate recombination occurs have yet to be clarified in sufficient detail.

One of the on-going issues that limit the application of organic solar cells is the degradation of device performance during their lifetime.⁴ Device efficiency has been shown to decrease with time, especially under illumination, and this detrimental effect is further accelerated when the

1
2
3 cells are operated in ambient conditions.⁵⁻¹¹ Practical devices will require a sustained efficiency
4
5 for up to 10 years and shall not be affected by external conditions such as oxygen, moisture, etc.
6
7 Possible solutions to this problem include more stable photoactive materials,¹² inverse
8
9 architectures,¹³ interfacial layers for improved charge extraction,¹⁴ as well as device
10
11 encapsulation.¹⁵ In addition, these factors must be considered in the context of low-cost and
12
13 high-throughput manufacturing. To identify and exploit the most effective architectures again
14
15 requires a fundamental understanding of the loss mechanisms which have so far limited device
16
17 lifetime and stability.
18
19
20
21
22

23 Several studies have examined the chemical and physical degradation of the photoactive layer
24
25 as well as the interfacial contacts where charge is extracted in these devices.^{8,16,17} The conjugated
26
27 polymers that are used in the photoactive layer are susceptible to photochemical modification in
28
29 the presence of water and can also undergo a reversible doping in the presence of oxygen while
30
31 under illumination. These two atmospheric contaminants can also react with the interfacial
32
33 layer(s) and charge extracting electrodes. All of these effects have been shown to reduce device
34
35 efficiency as reflected by a reduction in the measured short-circuit current and fill factor. In
36
37 addition, chemical and physical degradation of the photoactive layer can promote modification
38
39 of the interface at the charge collecting electrodes, which can be further accelerated for
40
41 photoactive layers prepared using low PCBM contents.¹⁸
42
43
44
45
46
47

48 Intensity modulated photocurrent spectroscopy (IMPS) is a powerful characterization
49
50 technique that has recently been shown to be an effective method for the investigation of charge
51
52 transport and carrier recombination in organic solar cells, particularly as related to device
53
54 stability.¹ Using this technique it is possible to separate the contributions of geminate and non-
55
56 geminate recombination since they occur on a different time scale. This opens a way to better
57
58
59
60

1
2
3 understand the effect of these processes on the device efficiency. Recently we demonstrated
4
5 using IMPS and its sister technique, intensity modulated photovoltage spectroscopy (IMVS), that
6
7 interfacial non-geminate recombination plays an important role in low efficiency of bulk
8
9 heterojunction organic solar cells.¹ Furthermore, it was found that the recombination rate actually
10
11 increased with device ageing and the illumination intensity,¹ which suggested that a large density
12
13 of interfacial states able to trap photogenerated carriers was formed under illumination. Similar
14
15 observations have been made recently by other authors using IMPS^{19,20} and related techniques
16
17 such as intensity-modulated scanning Kelvin probe microscopy²¹ and IMVS²² for organic bulk
18
19 heterojunction solar cells as well as for other solar cell types like perovskites.²³ An increase in
20
21 the recombination rate upon degradation and exposure to ambient air was also recently noted
22
23 using IMPS.²⁴
24
25
26
27
28
29

30 In this context it is important to better understand the nature of the states that are formed upon
31
32 degradation and augment the recombination losses. In the case of non-geminate recombination in
33
34 donor-acceptor materials, the recombining carriers are those that are formed upon dissociation of
35
36 primary excitons, that is, holes in the P3HT phase and electrons captured by the PCBM acceptor
37
38 phase. Using this argument, we suggested in our previous work that these sites could be located
39
40 either at the P3HT:PCBM internal heterojunction interface or at the Al contact where both P3HT
41
42 and PCBM domains come close to the contact.¹ Later, Luther and co-workers²⁴ attributed the
43
44 occurrence of non-geminate recombination to formation of certain deep traps inside the
45
46 photovoltaic layer. However, their treatment considered photogeneration, transport and
47
48 recombination inside the photovoltaic layer as a whole and so the exact location of those traps
49
50 within the photovoltaic layer could not be clarified. For instance, their model could not distinguish
51
52 between interfacial recombination at P3HT/PCBM bulk heterojunction and bulk recombination
53
54
55
56
57
58
59
60

1
2
3 inside, for instance, phase-segregated P3HT or PCBM grains. Very recently, Grey and co-
4
5 workers^{25,26} reported their results of intensity modulated photocurrent imaging of P3HT/PCBM
6
7 bulk heterojunction solar cells where they directly observed enhanced non-geminate
8
9 recombination rates at the interfaces between P3HT and PCBM domains, which were
10
11 presumably caused by formation of interfacial states that promoted recombination. However, the
12
13 origin of such states still remains unexplored.
14
15
16
17

18
19 In this work, we further explore this research direction and confirm, using a detailed analysis
20
21 of the IMPS data at various light intensities, that interfacial recombination indeed occurs at the
22
23 interfacial states at the P3HT/PCBM interface. These states are not involved in carrier extraction
24
25 and act as recombination centers only. Furthermore, the occurrence of these states is found to be
26
27 directly related to exposure of cells to atmospheric contaminants. Exclusion of atmospheric
28
29 exposure through encapsulation was effective in eliminating interfacial recombination, whereas
30
31 devices that were not encapsulated demonstrated a significant amount of interfacial
32
33 recombination that was dependent on the photoactive layer composition. Furthermore, it was
34
35 found that even a brief exposure of non-encapsulated devices to atmospheric conditions was
36
37 sufficient to form a significant number of interfacial states that continued to act as efficient
38
39 recombination centers and contributed to continuing degradation of the cell performance even
40
41 without any further atmospheric exposure. The devices with low PCBM loading ratio were
42
43 shown to suffer most from this effect thus suggesting the need of using higher PCBM loading
44
45 ratios to ensure the long term stability of bulk heterojunction solar cells.
46
47
48
49
50
51
52
53
54
55
56
57
58
59
60

2. Experimental

2.1. Materials

ITO-coated glass substrates (CEC20S, $\leq 20 \Omega \text{ sq}^{-1}$) from Präzisions Glass & Optik GmbH were cleaned in an ultrasonic bath with, sequentially, detergent deionized water (DI water), acetone and isopropyl alcohol, followed by UV ozone cleaning for 10 minutes. PEDOT:PSS (Bayer Baytron Co.), P3HT (98.5% regioregular from Sigma Aldrich Co.), and PCBM (Solenne BV Co.) were used as received without further purification.

2.2. Device fabrication

Bulk heterojunction solar cells were fabricated using an ITO/PEDOT:PSS/P3HT:PCBM/Al architecture. A PEDOT:PSS hole transport layer was spin-coated onto ITO and annealed in an oven at 120°C for 15 minutes prior to spin-coating the P3HT:PCBM photoactive layer. The ratio of the P3HT:PCBM photoactive layer was varied from 1:0.5 to 1:0.8 by varying the mass ratio of P3HT and PCBM dissolved in dichlorobenzene leading to films with a thickness of approximately 120 nm.²⁷ The total mass of the P3HT and PCBM was always 40 mg mL⁻¹. An aluminum cathode was evaporated on-top of the photoactive layer to complete the cell. The completed devices were annealed at 150°C for 30 minutes in an inert atmosphere. They were not exposed to ambient conditions at any time during fabrication. For some of the cells, a UV curable epoxy resin was used to encapsulate the devices. Devices were fabricated at the University of Strasbourg, France. Completed devices were placed in a vacuum sealed container and transported to the University of Western Ontario, Canada for IMPS measurements. However, the container used could not support high vacuum and therefore the cells were necessarily exposed to some atmospheric contamination during transportation. Upon arrival to

1
2
3 the University of Western Ontario, all cells were immediately placed in a nitrogen-purged glove
4
5 box or an Ar-purged environmental chamber and were not exposed to atmospheric conditions
6
7
8 again.
9

10 11 *2.3. Steady-state J-V measurements*

12
13
14 A solar simulator was used for AM 1.5 (100 mW cm⁻²) photocurrent measurements at the
15
16 University of Strasbourg, France. Photocurrent measurements at the University of Western
17
18 Ontario were performed using a 20 mW monochromatic 405 nm laser diode (LD1510, Power
19
20 technology). This light source was used to ensure consistency with IMPS measurements, which
21
22 were performed using the laser diode light source. The range of light intensities used was
23
24
25
26 3.07·10¹⁶ to 2.95·10¹⁷ photons·cm⁻²·s⁻¹, which corresponds to an incident power of 15 mW·cm⁻²
27
28 to 145 mW·cm⁻². Steady-state J-V measurements were collected using a PAR 263A potentiostat–
29
30 galvanostat (Princeton Applied Research) that was controlled using version 3.1 CorrWare
31
32 software (Scribner Associates Inc.). Ageing of the photovoltaic devices was done at room
33
34
35 temperature in a nitrogen purged glovebox for 30 days.
36
37
38

39 40 *2.4 Intensity modulated photocurrent measurements*

41
42
43 Intensity modulated photocurrent/photovoltage measurements were made using either a PAR
44
45 263A potentiostat–galvanostat (Princeton Applied Research) coupled with a Solartron 1250
46
47 frequency response analyzer or a stand-alone Solartron 1260 frequency response analyzer. The
48
49 dc light intensity was varied from 3.07·10¹⁶ to 2.95·10¹⁷ photons·s⁻¹·cm⁻², while the ac one was
50
51 kept constant at 3.07·10¹⁶ s⁻¹·cm⁻², which was determined to be small enough to ensure a linear
52
53 cell response. All measurements were performed in an Ar purged environmental chamber
54
55 equipped with an optical window.
56
57
58
59
60

3. Results and Discussion

3.1. Steady-state measurements of bulk heterojunction solar cells

A series of bulk heterojunction devices containing varying amounts of PCBM were fabricated and investigated using steady state current-voltage measurements as well as the non-steady state technique intensity modulated photocurrent spectroscopy. Mass ratios of P3HT to PCBM of 1:0.5, 1:0.6, 1:0.7, and 1:0.8 were used. It has been shown that low PCBM contents give rise to lower efficiencies than higher PCBM contents, with the optimal mass ratio being in the range of 1:0.8 to 1:1.²⁸ While efficiencies as high as 5 % can be obtained for the P3HT:PCBM system through judicious modification of the processing parameters, the majority of reports using P3HT with PCBM typically exhibit device efficiencies in the range of 2 – 3.5 %. For the photoactive layer compositions used in this work, device efficiencies in the range of 1.7 – 2.5 % were obtained under AM 1.5 solar simulator conditions immediately following device fabrication (see Table 1). The efficiencies were similar for both encapsulated and non-encapsulated devices. The lowest PCBM content films (1:0.5) exhibited the lowest efficiencies of 1.7 %, while all other compositions exhibited efficiencies of approximately 2.5%. The lower efficiency observed for the 1:0.5 P3HT:PCBM mass ratio is attributed to the inefficient formation of a percolation network throughout the film.

Shortly following the solar simulator measurements, but at a different location at the University of Western Ontario, London, Canada (which therefore required the cells to be packed into a transfer vessel and transported to this location, see Experimental section for further details), the devices were again measured using a monochromatic laser diode ($\lambda = 405$ nm) and their efficiencies were determined from the corresponding J-V plots. Measurements were made

using this light source because it was also used for the IMPS measurements that are discussed further below. The results are also presented in Table 1.

Table 1. Device parameters for bulk heterojunction devices measured shortly after fabrication at the University of Strasbourg (AM 1.5) and after the transportation to the University of Western Ontario (Laser Diode)

P3HT:PCBM	Encapsulated				Non-Encapsulated			
	1:0.5	1:0.6	1:0.7	1:0.8	1:0.5	1:0.6	1:0.7	1:0.8
AM 1.5								
$j_{sc} / \text{mA cm}^{-2}$	6.78	8.24	7.41	6.92	7.41	8.66	8.49	7.47
V_{oc} / V	0.54	0.53	0.56	0.53	0.49	0.53	0.51	0.56
Efficiency / %	1.95	2.36	2.45	2.16	1.73	2.51	2.4	2.46
Fill Factor / %	53.2	53.8	59.6	59.8	47.5	55.2	55.8	59.2
Laser Diode								
$j_{sc} / \text{mA cm}^{-2}$	4.21	6.52	5.58	6.69	0.532	0.407	1.41	4.17
V_{oc} / V	0.52	0.50	0.54	0.56	0.42	0.38	0.43	0.46
Efficiency / %	0.99	1.60	1.59	1.86	0.04	0.05	0.15	0.67
Fill Factor / %	51.9	55.8	60.4	57.1	18.8	33.3	27.8	39.4

One can see from the table that encapsulated devices showed similar efficiencies when measured shortly following fabrication and after the transportation. A certain decrease in the efficiency when using the monochromatic laser diode was most likely due to a shorter wavelength of the laser diode light. However, non-encapsulated devices showed a substantial reduction in efficiency that was dependent on PCBM content in the films. The cell efficiency was also found to decrease after further aging for 30 days in the dark (Table 2) despite the fact that the cells were stored in inert atmosphere in a nitrogen-filled glove box during all this time.

Table 2. Device parameters for bulk heterojunction devices measured after aging in inert atmosphere at the University of Western Ontario.

P3HT:PCBM	Non-Encapsulated (aged)			
	1:0.5	1:0.6	1:0.7	1:0.8
Laser Diode				
$j_{sc} / \text{mA cm}^{-2}$	0.202	0.454	0.897	2.27
V_{oc} / V	0.48	0.42	0.44	0.54
Efficiency / %	0.01	0.03	0.06	0.21
Fill Factor / %	10.4	20.6	18.9	19.8

This trend is also illustrated in Fig. 1 that shows J-V plots of bulk heterojunction devices for two P3HT:PCBM mass ratios measured after transportation to the University of Western Ontario. The cells with other P3HT:PCBM mass ratios showed similar behavior (see Supporting Information). Curves (1) and (2) were measured right upon receiving the devices and correspond to encapsulated and non-encapsulated cells, respectively, whereas curve (3) corresponds to a non-encapsulated device that was aged for 30 days but without further exposure to atmospheric conditions.

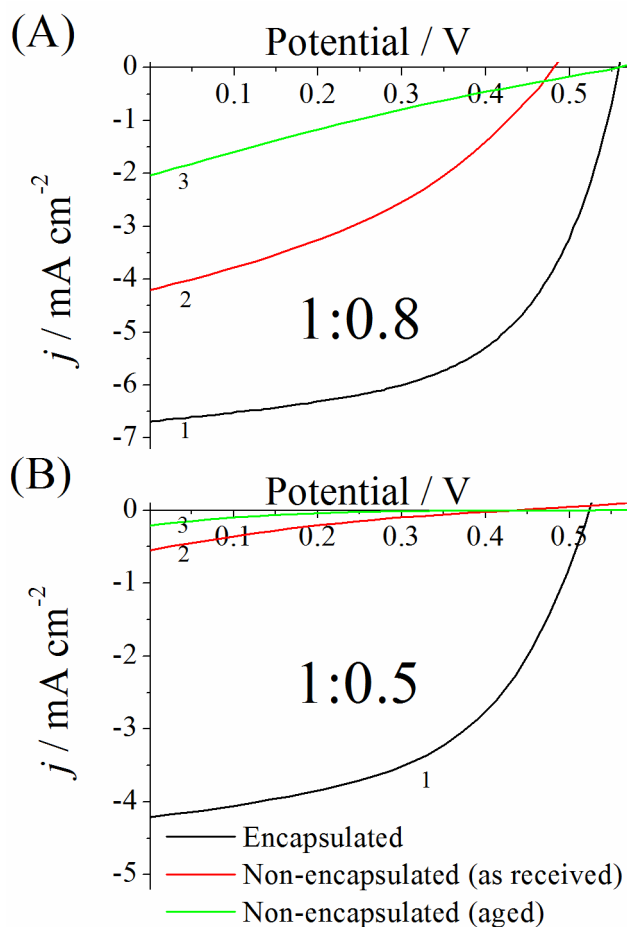


Figure 1. J-V plots of bulk heterojunction devices containing a P3HT:PCBM mass ratio of (A) 1:0.8 and (B) 1:0.5 measured using a 405 nm laser diode at the University of Western Ontario. The *dc* light intensity was $1.62 \cdot 10^{17} \text{ s}^{-1} \text{ cm}^{-2}$. Curves (1) and (2) correspond to encapsulated and non-encapsulated as-received devices, whereas curve (3) corresponds to non-encapsulated device that was aged for 30 days but without further exposure to atmospheric conditions.

Therefore, the data show that encapsulation plays a very significant role in the device efficiency. Whereas all devices showed comparable efficiencies right after fabrication, devices that were not encapsulated exhibited a substantial decrease in efficiency upon transportation compared to

1
2
3 devices that were encapsulated. The effects were especially severe for such parameters as the
4
5 short-circuit current density j_{SC} and fill factor. Therefore, the reduction in the cell efficiency
6
7 observed upon transportation for non-encapsulated cells should be related to the exposure to
8
9 atmospheric contaminants such as oxygen and moisture that could not be completely eliminated
10
11 during transportation. Furthermore, even though all devices received at the University of
12
13 Western Ontario were continuously stored in a glovebox under nitrogen upon their delivery
14
15 without further exposure to atmospheric contaminants, non-encapsulated cells continued to
16
17 undergo further deterioration of their performance, as opposed to encapsulated cells.
18
19
20
21

22
23 It has been shown that atmospheric oxygen or moisture, if present, are able to penetrate into
24
25 the photoactive layer through grain boundaries and pinholes present in the aluminum cathode
26
27 layer.⁸ Our data suggest that even short exposure to these contaminants is sufficient to modify
28
29 the photovoltaic layer in such a way as to cause continuous and irreversible degradation. One
30
31 possible mechanism of such effect may be formation of a large number of interfacial states inside
32
33 the photovoltaic layer due to reactions with oxygen and moisture, especially at the grain
34
35 boundaries. Such interfacial states, if present, would strongly enhance the rate of the interfacial
36
37 recombination and thus decrease the cell efficiency. In order to investigate this hypothesis, we
38
39 performed non-steady state intensity modulated photocurrent (IMPS) measurements since IMPS
40
41 is one of the most powerful techniques for studies of the interfacial recombination in various
42
43 photovoltaic materials.
44
45
46
47
48
49
50
51
52
53
54
55
56
57
58
59
60

1
2
3
4
5
6
7
8
9
10
11
12
13
14
15
16
17
18
19
20
21
22
23
24
25
26
27
28
29
30
31
32
33
34
35
36
37
38
39
40
41
42
43
44
45
46
47
48
49
50
51
52
53
54
55
56
57
58
59
60

3.2. Intensity modulated photocurrent spectroscopy (IMPS) of encapsulated and non-encapsulated devices

Figure 2 presents typical IMPS plots obtained in short-circuit conditions at the same light intensity for as-received encapsulated cell and non-encapsulated cells, as well as non-encapsulated cell upon ageing in nitrogen atmosphere for 30 days. Similar data were obtained for other cells and light intensities (see the complete set of data in the Supporting Information). The IMPS spectra are given both in Nyquist and Bode plot representation, that is, on the complex plane and as separated dependencies of the real and imaginary components of the photocurrent on the light modulation frequency. An important difference is immediately seen between encapsulated and non-encapsulated cells: the spectra for non-encapsulated cell show characteristic arcs in quadrant I of the complex plane (Nyquist representation) that become more pronounced upon ageing, whereas the spectrum for encapsulated cell does not show this feature. In the Bode representation, the imaginary component of the ac photocurrent for the encapsulated cell (curve 1) remains negative at all modulation frequencies, whereas the imaginary components for non-encapsulated cells (curves 2 and 3) change the sign and become positive at lower frequencies (photocurrent leads the light intensity). Such arcs as well as corresponding positive phase shifts are typical manifestations of the occurrence of interfacial recombination.^{1,29-34} All non-encapsulated cells demonstrated such arcs in our measurements, whereas all encapsulated cells lacked this feature. Therefore, we must draw a very important conclusion that encapsulation appeared to be a very effective measure to prevent the occurrence of interfacial recombination in bulk heterojunction devices. On the other hand, even brief exposure to atmospheric contaminants during device transportation was sufficient to cause the occurrence of pronounced interfacial recombination in our devices, as evidenced by IMPS data.

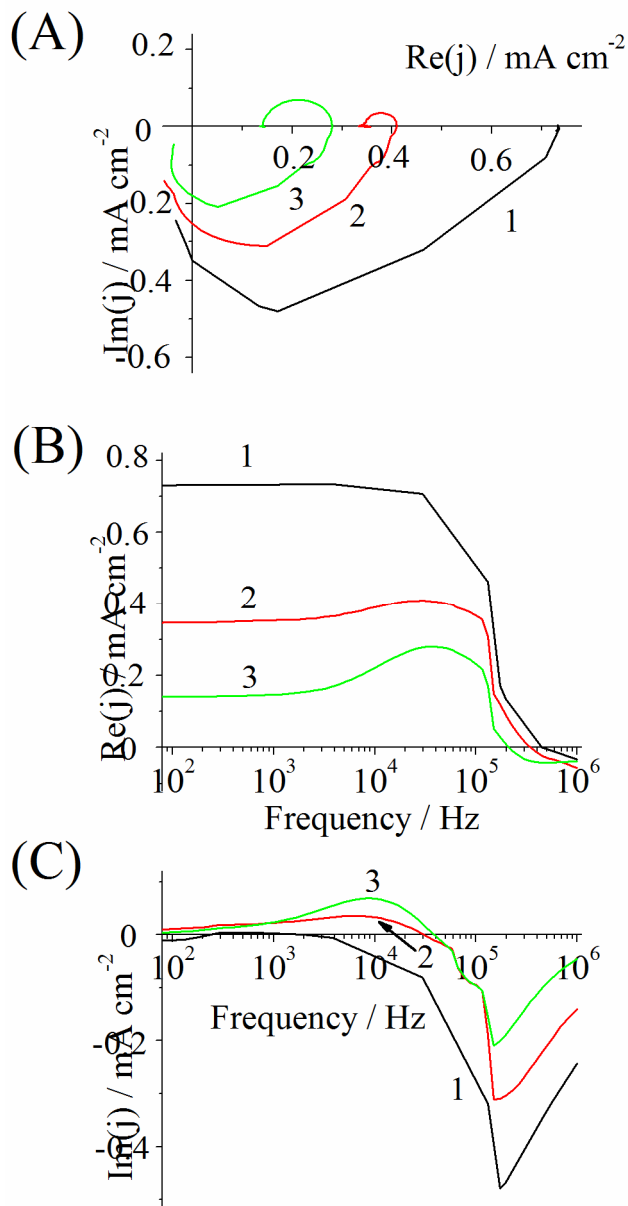


Figure 2. Typical IMPS spectra in (A) Nyquist and (B,C) Bode plot representation obtained in short-circuit conditions for (1) as-received encapsulated cell and non-encapsulated cell both (2) as-received and (3) upon ageing in nitrogen atmosphere for 30 days. The P3HT:PCMB ratio was 1:0.8 and the dc light intensity was $1.62 \cdot 10^{17} \text{ s}^{-1} \text{ cm}^{-2}$.

The occurrence of interfacial recombination in non-encapsulated devices upon exposure to atmospheric contaminants can explain a pronounced reduction in the short-circuit current density

1
2
3 as revealed by the data of Tables 1 and 2. In IMPS measurements, the short-circuit current
4
5 density measured under continuous illumination is represented by the low frequency limit of the
6
7 ac photocurrent ReJ_0 . It can be evaluated, for example, from the low-frequency plateaus in Fig.
8
9 2B. One can see that the occurrence of interfacial recombination in non-encapsulated devices
10
11 decreases this parameter significantly thus indicating additional losses that occur in the device
12
13 due to interfacial recombination.
14
15

16
17
18 Figure 2 curve 3 shows the IMPS data for the same cell as in curve 2 but measured following
19
20 aging in a controlled glovebox environment that limited further atmospheric exposure. One can
21
22 see that the aged cells show a reduction in both their high frequency and low frequency values
23
24 for the real component of the photocurrent indicating both a reduction in the number of
25
26 generated charge carriers and their poorer extraction with aging (see below for more discussion).
27
28 This is consistent with the results of the steady-state measurements. Also, the frequency at the
29
30 maximum for the imaginary photocurrent has shifted to a higher frequency for the aged cell in
31
32 comparison to the as-received cell. This indicates that the reason for the decrease in performance
33
34 upon cell aging is an increase in the rate of interfacial recombination. The same fact was
35
36 observed in our previous work.¹ The size of the characteristic arc for the aged cell is much larger
37
38 and the ReJ_0 value is much lower indicating a further increase in the fraction of charge carriers
39
40 that are lost to interfacial recombination.
41
42
43
44
45
46

47
48 Importantly, this increase in the recombination losses in aged cells occurred even without
49
50 further exposure to atmospheric contaminants. This fact highlights the importance of
51
52 encapsulation to prevent the recombination losses in bulk heterojunction devices. Furthermore,
53
54 since IMPS spectra are sensitive to the presence of interfacial states and can detect interfacial
55
56 recombination, IMPS can be used as a powerful diagnostic tool to predict the performance of
57
58
59
60

1
2
3 organic solar cells. All devices in this study that initially showed the presence of interfacial states
4 as indicated by characteristic semicircle arcs in the I quadrant of the IMPS spectra demonstrated
5 deterioration of their performance due to enhanced interfacial recombination, even without
6 further exposure to atmospheric contaminations.
7
8
9
10
11

12 13 14 *3.3. The effect of the light intensity*

15
16
17 Figure 3 presents typical IMPS spectra in the Nyquist and Bode plot representations obtained
18 for a non-encapsulated device at different *dc* light intensities for a 1:0.7 P3HT:PCBM mass ratio.
19 The cells with other P3HT:PCBM mass ratios showed similar results (See Table 3). The IMPS
20 plots follow similar trends to those observed with increasing *dc* light intensity in our previous
21 study.¹ Specifically, the maximum of the imaginary photocurrent in quadrant 1 shifts to higher
22 frequencies with increasing *dc* light intensity as shown in Figure 3C. The frequency at the
23 maximum of the imaginary photocurrent is represented by ω^* and corresponds to the pseudo first
24 order rate constant for interfacial recombination.
25
26
27
28
29
30
31
32
33
34
35
36
37
38
39
40
41
42
43
44
45
46
47
48
49
50
51
52
53
54
55
56
57
58
59
60

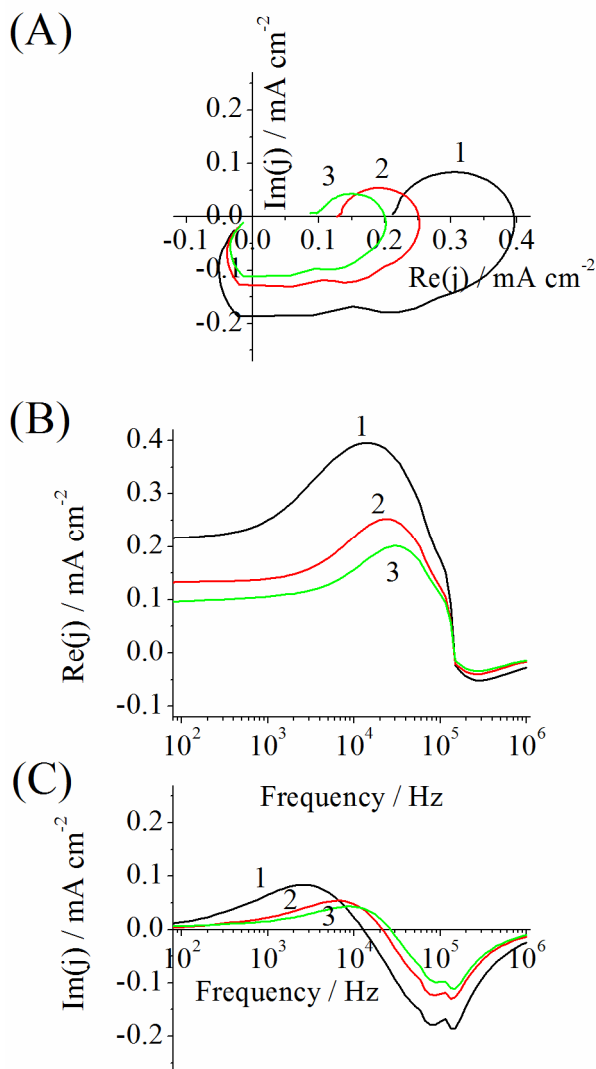
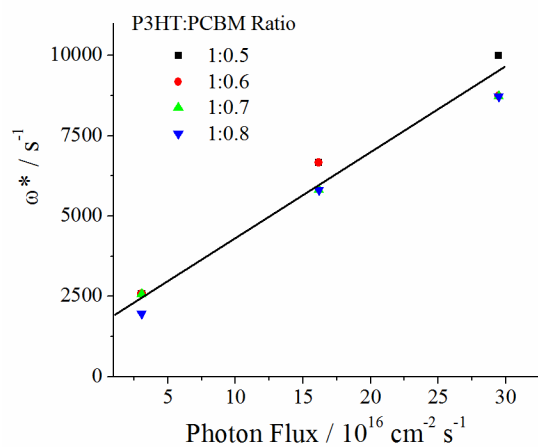


Figure 3. Typical IMPS spectra obtained in short-circuit conditions for a P3HT:PCBM ratio of 1:0.7 in (A) Nyquist and (B,C) Bode plot representation. The *dc* light intensity used was (1) $3.07 \cdot 10^{16}$, (2) $1.62 \cdot 10^{17}$, and (3) $2.95 \cdot 10^{17} \text{ s}^{-1} \cdot \text{cm}^{-2}$.

Figure 4 shows the frequency corresponding to the maximum of the imaginary photocurrent in quadrant I for all cells as a function of *dc* light intensity. It can be seen that the recombination rate increases with increasing *dc* light intensity for all cells, but it does not appear to show a significant variation or dependence on the PCBM content. It is important to point out that the

1
2
3 pseudo-first order rate constant ω^* implicitly includes the majority carrier concentration.
4
5 Therefore, these data suggest that recombination involves not only photogenerated minority
6 carriers but photogenerated majority carriers (holes) as well. These carriers should be located in
7
8 the p-type P3HT phase. Normally, photogenerated majority carriers are rapidly swept away by
9
10 the electric field; however, the carrier mobilities in conjugated organic semiconductors such as
11
12 P3HT could be lower and thus some photogenerated majority carriers may be trapped near the
13
14 interface and contribute to the recombination with photogenerated electrons. Our data suggest
15
16 that this is a predominant recombination mechanism since the values of the recombination rate
17
18 constant under illumination are significantly higher than those in the dark (found as the
19
20 extrapolation of the recombination rate to zero light intensity, Figure 4).
21
22
23
24
25
26
27
28
29



30
31
32
33
34
35
36
37
38
39
40
41
42
43
44
45 **Figure 4.** The value of the rate constant for recombination ω^* for all the P3HT:PCBM mass
46 ratios for as received devices as a function of the *dc* light intensity. The line is not a fit and is a
47
48 guide for the eyes.
49
50

51
52 The values of the ac photocurrent also follow the trend (Fig. 3). An increase in the *dc* light
53
54 intensity results in a reduction in both the real and imaginary components of the photocurrent
55
56 over a wide frequency range. This means that more carriers are lost to recombination at higher
57
58
59
60

1
2
3 light intensities again suggesting the involvement of photogenerated majority carriers trapped in
4 P3HT phase. Importantly, the photocurrent decreases over a wider frequency range than those
5 attributed to interfacial recombination. This fact suggests that trapping of photogenerated
6 majority carriers occurs not only near the interface but also in the bulk of P3HT phase and
7 contribute to both interfacial and bulk recombination losses.
8
9

10
11
12
13
14
15
16 The independence of ω^* of the PCBM content for a given dc light intensity suggests that the
17 rate constant for the interfacial recombination does not depend on the PCBM or P3HT
18 concentrations. However, the short-circuit current densities for non-encapsulated devices do
19 exhibit a dependence on the PCBM content as observed in their steady-state J-V plots (Table 1
20 and Supporting Information), with films containing a greater fraction of PCBM showing higher
21 efficiencies. It could be expected that the recombination rate constant would increase for
22 decreasing PCBM contents if interfacial recombination were occurring at the PCBM/Al
23 interface, which would lead to a dependence of the recombination rate constant on the PCBM
24 content in the active layer and at the interface. This is discussed in the next Section.
25
26
27
28
29
30
31
32
33
34
35
36
37

38 *3.3. The effect of the PCBM content*

39
40
41
42 Figure 5 shows the IMPS spectra for P3HT:PCBM films with increasing ratios of PCBM
43 content in the photoactive layer. Several trends can be observed in these figures. The Bode plot
44 in Figure 5B shows that for increasing PCBM content, the low frequency portion of the real
45 photocurrent is greater in magnitude, which is similar to the trend observed in the steady state J-
46 V plots (Figure 1) above. As well, Figure 5C shows that ω^* does not vary significantly with the
47 P3HT:PCBM ratio, which would suggest that an increase in the rate constant for recombination
48 with decreasing PCBM content cannot explain the decrease in device efficiency. The shape of
49
50
51
52
53
54
55
56
57
58
59
60

1
2
3 the IMPS spectra (Fig 5A) in the first quadrant shows that cells with higher PCBM content
4
5 exhibit a smaller semicircle than those with lower PCBM content. This is indicative of reduced
6
7 recombination in the devices, but this is not accompanied by a change in the value of ω^* as
8
9 observed in Figure 5C.
10
11
12
13
14
15
16
17
18
19
20
21
22
23
24
25
26
27
28
29
30
31
32
33
34
35
36
37
38
39
40
41
42
43
44
45
46
47
48
49
50
51
52
53
54
55
56
57
58
59
60

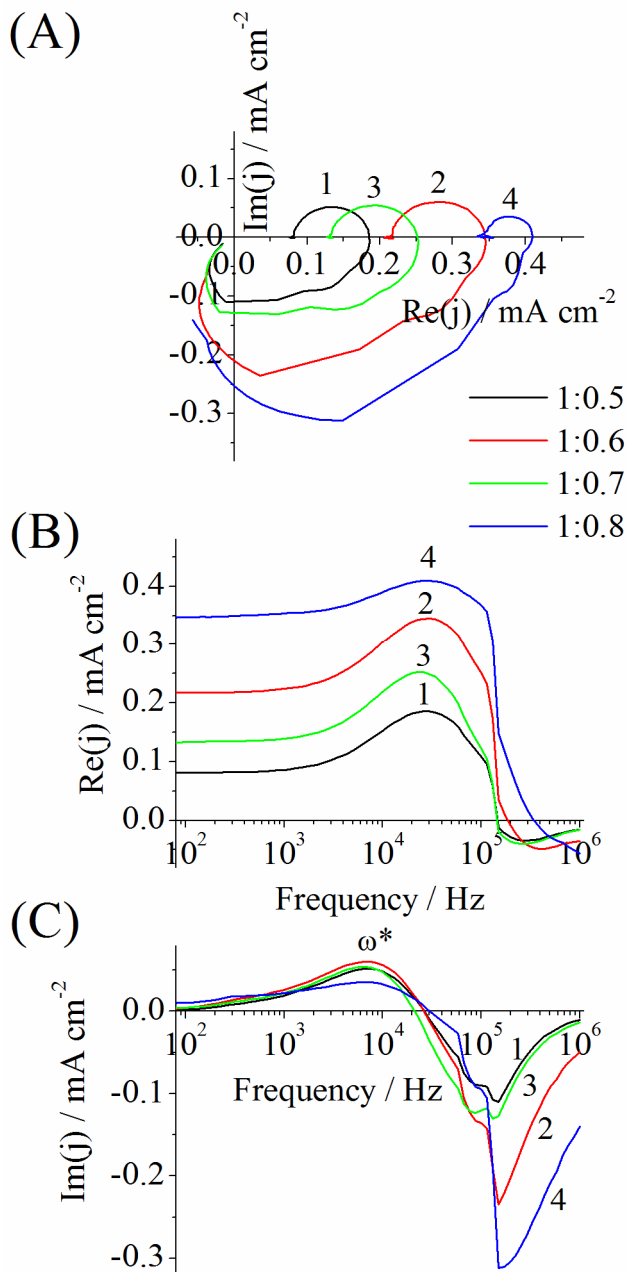


Figure 5. Experimental IMPS spectra for as received devices obtained in short-circuit conditions for P3HT:PCBM ratios of (1) 1:0.5, (2) 1:0.6, (3) 1:0.7, and (4) 1:0.8 in (A) Nyquist and (B,C) Bode plot representation. The dc light intensity for all spectra was $1.62 \cdot 10^{17} \text{ s}^{-1} \cdot \text{cm}^{-2}$.

Figure 6 shows the normalized low frequency portions of the IMPS spectra for a series of P3HT:PCBM cells at a light intensity of $1.62 \cdot 10^{17} \text{ s}^{-1} \cdot \text{cm}^{-2}$. Normalizing the data allows a

comparison between the size and shape of the spectra, which are due to differences in interfacial recombination. One can see that the semicircles in the first quadrant increase in size with decreasing PCBM content, which indicates that an increasing number of charge carriers are lost to interfacial recombination for lower PCBM containing films. To further understand the role of interfacial recombination it is useful to define three parameters as indicated in Figure 6. The three parameters are the (1) high frequency intercept g_{ac} , (2) the low frequency intercept ReJ_0 , and (3) the frequency corresponding to the maximum of the imaginary photocurrent in the first quadrant ω^* .

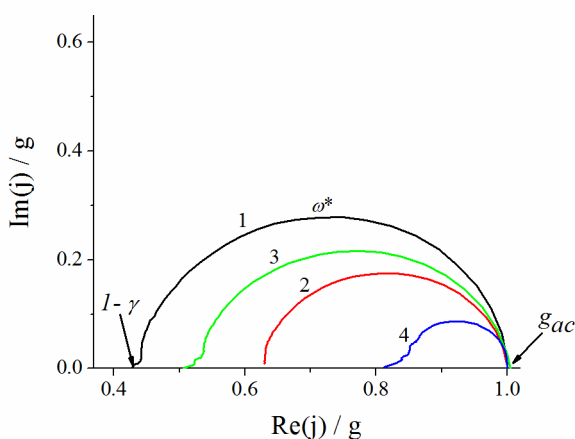


Figure 6. Normalized IMPS spectra for as received devices obtained at short-circuit conditions for P3HT:PCBM ratios of (1) 1:0.5, (2) 1:0.6, (3) 1:0.7, and (4) 1:0.8. The *dc* light intensity for all spectra was $1.62 \cdot 10^{-17} \text{ s}^{-1} \cdot \text{cm}^{-2}$. The high frequency intercept g_{ac} , low frequency intercept $I-\gamma$ and the maximum of the imaginary photocurrent ω^* are indicated.

The high frequency intercept is determined by the point in the complex plane plots of Fig. 5A at which the imaginary photocurrent crosses over from quadrant IV to quadrant I. It can also be

1
2
3 determined as the maximum value of the real photocurrent, e.g., as in Fig. 5B. This parameter is
4 indicated in Figure 6 as g_{ac} , which is unity in the normalized plots, and represents the maximum
5 attainable photocurrent if no interfacial recombination were occurring. The next parameter is the
6 frequency that corresponds to the maximum for the imaginary photocurrent in quadrant I,
7 indicated by ω^* in Figure 6. The final parameter is the real photocurrent ReJ_0 measured at low
8 frequency, which represents the situation where the steady-state photocurrent would be
9 measured. As has been already discussed, it can be also determined from the low-frequency
10 plateau on the frequency dependence of the real component of the photocurrent (e.g., Fig. 5B). In
11 the normalized plots, this is the fraction of charge carriers that are not lost to interfacial
12 recombination and are extracted at the electrode. This parameter can be represented by the
13 product $g_{ac}(1 - \gamma)$, where γ denotes the fraction of charge carriers that recombine. A smaller value
14 of $g_{ac}(1 - \gamma)$ indicates a greater number of charge carriers that are lost to interfacial
15 recombination. The parameters ReJ_0 , g_{ac} , and $g_{ac}(1 - \gamma)$ are related through the following
16 expression:
17
18
19
20
21
22
23
24
25
26
27
28
29
30
31
32
33
34
35
36

$$ReJ_0 = g_{ac}(1 - \gamma), \quad (1)$$

37
38 which can be arranged in the following form:
39
40
41
42

$$(1 - \gamma) = ReJ_0 / g_{ac} \quad (2)$$

43
44
45
46
47 The values of this parameter are given in Table 3 along with the experimental values for the
48 low frequency limit of the photocurrent ReJ_0 , high frequency limit of the photocurrent g_{ac} , and
49 the frequency corresponding to the maximum of the imaginary photocurrent in the first quadrant
50 ω^* determined from the IMPS plots.
51
52
53
54
55
56
57
58
59
60

Table 3. Values for the low frequency limit ReJ_0 , the high frequency limit g_{ac} , the frequency at the maximum of the imaginary photocurrent in the first quadrant ω^* and the fraction of the carriers captured at the interfacial states γ determined from the IMPS plots.

	As received				Aged			
P3HT:PCBM	1:0.5	1:0.6	1:0.7	1:0.8	1:0.5	1:0.6	1:0.7	1:0.8
$g_{ac} / \text{mA cm}^{-2}$	0.186	0.342	0.250	0.408	0.202	0.238	0.262	0.280
$ReJ_0 / \text{mA cm}^{-2}$	0.082	0.218	0.133	0.348	0.0110	0.0780	0.090	0.141
ω^* / s^{-1}	6660	6660	5800	5800	8730	8730	8730	8730
γ	0.56	0.37	0.48	0.17	0.94	0.68	0.65	0.50

It is clear from Figure 6 and Table 3 that that the value $ReJ_0 = g_{ac}(1 - \gamma)$ increases with the amount of PCBM in the film indicating that the contribution of the interfacial recombination increases at low PCBM contents, which is reflected in a lower device efficiency. Therefore, we conclude that while the rate of interfacial recombination per se does not depend significantly on the PCBM content, as suggested by the independence of the parameter ω^* , an increase in the PCBM content reduces the recombination losses by decreasing the fraction γ of photogenerated carriers trapped at the interfacial states. An obvious explanation for this effect is that an increase in the PCBM content enhances the charge separation and extraction, which is a competing process to the interfacial recombination. Incidentally, this is an indication of the localization of interfacial recombination at the P3HT/PCBM interface. This is explored in detail in the next section. Furthermore, an increase in the PCBM content increases the generation current g_{ac} thus again suggesting an increase in the efficiency of exciton dissociation with the PCBM content or improved bulk transport.

These conclusions are also supported by the observations of the changes in the steady-state J-V curves with PCBM content (Tables 1 and 2). One can see that despite an overall decrease in the

1
2
3 efficiency, the short-circuit current density and the fill factor were still increasing with the
4
5 PCBM content for both as-received and aged cells. However, aged cells show a significantly
6
7 decreased value of the short-circuit current density compared to the as-received cells, with the
8
9 differences becoming more pronounced at higher PCBM contents. This correlates well with the
10
11 behavior of parameters $g_{ac}(1 - \gamma)$ and ReJ_0 derived from IMPS spectra (Table 3) and can be also
12
13 explained by enhanced charge separation and extraction in the photovoltaic layer. Importantly,
14
15 encapsulated devices as well as as-prepared non-encapsulated devices before transportation
16
17 (Table 1) did not exhibit such dependence on the PCBM content suggesting that differences in
18
19 phase segregation, morphology or interfacial mixing between the two materials is not the origin
20
21 of the observed dependence of the device efficiency on the PCBM content. Rather, the latter
22
23 should be attributed to the formation of the interfacial states upon exposure to the atmospheric
24
25 contaminants and competition between carrier separation/extraction and their capture at the
26
27 interfacial states. The same mechanism should be responsible for the observed changes in the fill
28
29 factor.
30
31
32
33
34
35
36

37 The open circuit voltage (Tables 1 and 2) does not vary significantly with PCBM content and
38
39 even increases slightly for aged cells. The relative independence of the open circuit voltage with
40
41 the PCBM content can be expected as its value is a function of the difference between the
42
43 LUMO level of the PCBM and HOMO level of P3HT, which does not change with variations of
44
45 the PCBM content. A slight increase in V_{oc} with aging can be attributed to an increased shunt
46
47 resistance of the film that occurs due to film degradation.¹⁰
48
49
50
51
52
53
54
55
56
57
58
59
60

1
2
3 3.4. Analysis of the recombination mechanism from parameters derived from IMPS
4
5 *measurements*
6

7
8
9 To better understand which interface is primarily responsible for the occurrence of the
10 interfacial recombination, PCBM/Al or P3HT/PCBM, two separate models are used to interpret
11 the IMPS spectra that correspond to different interfaces where recombination could occur. In
12 both models it is important to state that we are discussing the trapping of an electron at an
13 interfacial state. In this case, recombination of photoexcited electrons cannot occur at the
14 interfacial states formed between P3HT and the aluminum cathode, as P3HT is a hole majority
15 carrier with low exciton dissociation efficiency on its own and will have no or very few free
16 photogenerated electrons. Therefore, electron recombination from P3HT at the aluminum
17 cathode cannot explain the significant amount of charge that is being generated and collected in
18 our measurements. The two remaining interfaces where interfacial recombination can occur are
19 the P3HT/PCBM interface or the PCBM/Al interface. These two separate cases are illustrated
20 below in Figure 7.
21
22
23
24
25
26
27
28
29
30
31
32
33
34
35
36
37
38
39
40
41
42
43
44
45
46
47
48
49
50
51
52
53
54
55
56
57
58
59
60

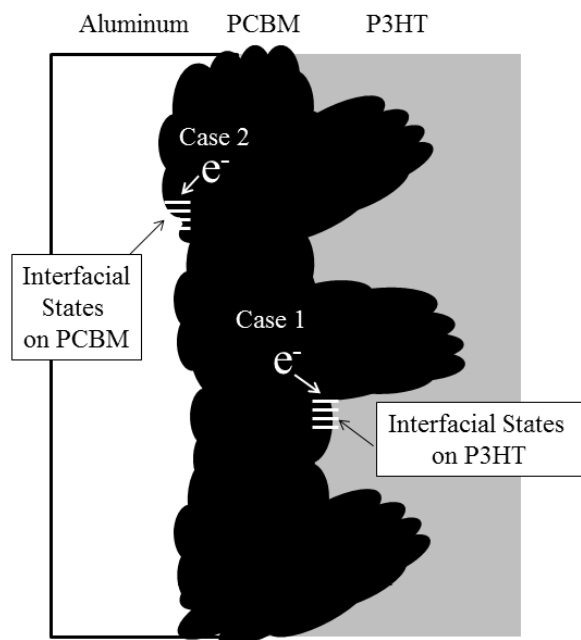


Figure 7. Schematic showing the possible interfaces where interfacial recombination may occur in a bulk heterojunction P3HT:PCBM device.

Case 1: No extraction from interfacial states

In case 1, the interfacial states responsible for the recombination are assumed to be located at the P3HT/PCBM interface. Therefore, all carriers trapped at the interfacial states recombine and cannot be extracted. In this case, the low frequency intercept of the real component of the photocurrent $ReJ_0 = g_{ac}(1 - \gamma)$ will correspond to carriers that escape trapping at the interfacial states and are extracted directly at the PCBM/Al interface. The corresponding fraction of carriers that escape trapping and recombination will be equal to $1 - \gamma$ as described above. Figure 8A plots the experimental values for the low and high frequency intercepts in quadrant I as a function of the PCBM content for aged cells (data for as-received cells demonstrated similar behavior and are not shown), while Figure 8B plots the corresponding values of $1 - \gamma$ for as-received and aged cells.

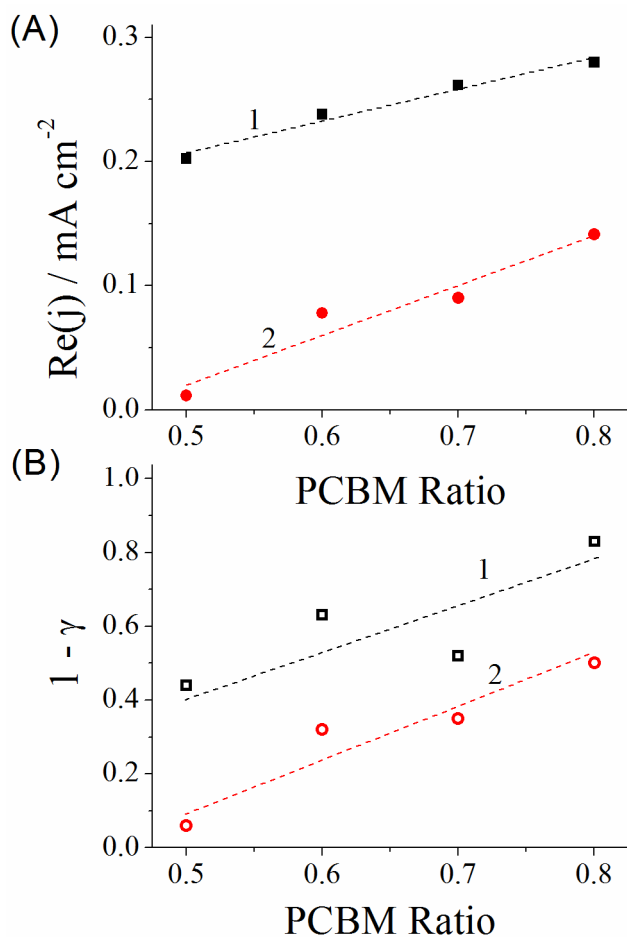


Figure 8. (A) Values for the (1) high frequency intercept g_{ac} and the (2) low frequency intercept ReJ_0 for aged cells as a function of PCBM content in the film. (B) Fraction of charge carriers collected at the contacts $1 - \gamma$ as a function of PCBM content for (1) as-received cells and (2) aged cells. A light intensity of $1.62 \cdot 10^{17} \text{ s}^{-1} \text{ cm}^{-2}$ was used.

From Fig. 8A one can see that g_{ac} decreases with decreasing PCBM content indicating that carriers are not being generated as efficiently and/or being lost to bulk recombination as the PCBM content in the film is decreased. However, examination of the value of ReJ_0 in Figure 8A shows that its value decreases much more rapidly compared to g_{ac} with decreasing PCBM

1
2
3 content. The difference in the slope for the values of ReJ_0 compared to g_{ac} demonstrates that
4
5 losses due to interfacial recombination are dramatically enhanced for devices with low PCBM
6
7 content.
8
9

10
11 Figure 8B plots the value of $I - \gamma$, which represents the fraction of photogenerated charges that
12
13 are extracted at the electrode. One can see that this value increases significantly with an increase
14
15 in the PCBM content. This indicates enhanced carrier extraction in the device. At the same time,
16
17 as was shown above, the pseudo first order rate constant for interfacial recombination did not
18
19 depend or showed only a slight dependence on the PCBM content in the film. Taken together,
20
21 these two facts indicate that an increase in the cell efficiency at elevated PCBM contents is not
22
23 due to suppression of interfacial recombination but rather originates from enhanced carrier
24
25 extraction at the PCBM/Al interface.
26
27
28
29
30

31 This mechanism is further corroborated by the light intensity dependencies of parameters $I - \gamma$
32
33 and ω^* . As has been discussed above (see Figure 4), the parameter ω^* that represents in this
34
35 model the pseudo-first order recombination rate constant increases significantly with the light
36
37 intensity, whereas the parameter $(I - \gamma)$ was found to be virtually independent of the light
38
39 intensity. The light intensity dependence of ω^* was attributed to the majority carriers (holes)
40
41 trapped in the P3HT phase. Therefore, these facts suggest that carrier extraction indeed should
42
43 occur at the PCBM/Al interface where no contribution from carriers trapped in P3HT could be
44
45 expected, whereas the recombination should occur at the internal PCBM/P3HT interface between
46
47 phase segregated P3HT and PCBM domains.
48
49
50
51
52

53
54 The rate of interfacial recombination increases with aging, which suggests either further
55
56 chemical modification of the active layer or morphological changes in the film/at the interfaces.
57
58
59
60

1
2
3 While oxygen can modify the conjugated polymer under illumination, this process does not
4 occur in the dark.¹⁶ These devices were stored in a glovebox in the dark during aging and
5 photochemical modification is not likely in this case. At the same time, our results do show that
6 exposure to oxygen and moisture triggers certain processes at the interfaces/grain boundaries
7 between the P3HT and PCBM phases that promote continuing formation of interfacial states
8 even without further atmospheric exposure. The interfacial states then start to trap more
9 photoexcited carriers thus increasing the recombination losses. The specific mechanisms may
10 involve chemical modification of P3HT and/or PCBM at the grain boundaries between the P3HT
11 and PCBM rich domains; however, their clarification requires further studies.
12
13
14
15
16
17
18
19
20
21
22
23
24

25 It has been shown that the addition of a fullerene (C_{60}) layer between the photoactive layer and
26 cathode led to more reproducible bulk heterojunction organic photovoltaic devices.³⁵ This
27 increase in reproducibility was attributed to the formation of a more stable interface between the
28 photoactive layer and cathode material. It has also been shown that a C_{60} layer is able to prevent
29 the diffusion of oxygen into the active layer, which would help to reduce degradation and
30 interfacial recombination.⁸ Taken into consideration our results presented here, it is possible that
31 such an interfacial C_{60} layer can also modify the PCBM/Al interface and improve carrier
32 extraction at it. It could be expected that stable bulk heterojunction films with lower PCBM
33 contents could be prepared if an interfacial layer between the photoactive layer and cathode was
34 incorporated and the morphology did not change significantly. This may be a useful
35 consideration when evaluating alternative acceptor materials to exclude interfacial effects. In
36 addition, this may provide new opportunities to engineer the morphology and composition of the
37 photoactive layer using new materials, if high loading ratios are not required.
38
39
40
41
42
43
44
45
46
47
48
49
50
51
52
53
54
55
56
57
58
59
60

1
2
3 *Case 2: All carriers are extracted through interfacial states only*
4
5

6
7 In the previous case it was assumed that carriers cannot be extracted once they become trapped
8
9 at an interfacial site and the charge transfer occurs directly from PCBM to Al without
10
11 involvement of interfacial states. Case 2 considers the opposite situation where photogenerated
12
13 charge carriers are extracted through interfacial states only.³⁶ In this case there is a competition
14
15 between charge carrier recombination and charge carrier transfer from the interfacial state and
16
17 the interfacial recombination would occur at the PCBM/Al interface where there is the
18
19 possibility that there would be a competition between charge carrier recombination in PCBM or
20
21 extraction at the aluminum electrode. Therefore, the parameter ω^* will no longer be simply a
22
23 pseudo first order recombination rate constant and should incorporate two separate components
24
25 that include a rate constant for charge transfer k_{tr} from the interfacial states to the Al electrode
26
27 along with a rate constant for interfacial recombination k_{rec} . The values of these two rate
28
29 constants can be determined from the experimental IMPS plots by taking the sum of the charge
30
31 transfer rate constant and the interfacial recombination rate constant and equating them to ω^* as
32
33 shown in equation 3:
34
35
36
37
38
39

40
41
$$\omega^* = k_{tr} + k_{rec} \quad (3)$$

42
43
44
45

46 where k_{tr} is the rate constant for charge transfer and k_{rec} is the rate constant for interfacial
47
48 recombination. Separation of these two components requires knowledge of the low frequency
49
50 intercept of the real photocurrent, which represents the fraction of electrons that are collected at
51
52 the electrode and do not recombine. Since case 2 assumes that all carriers are extracted through
53
54 interfacial states, this fraction for this model is expressed as:
55
56
57
58
59
60

$$ReJ_0 = g_{ac} \cdot k_{tr} / (k_{tr} + k_{rec}) \quad (4)$$

Using Equations 3 and 4, it is possible to determine k_{tr} from k_{rec} from the high and low frequency intercepts along with the frequency at the maximum of the imaginary component of the photocurrent for quadrant I. The corresponding values of k_{tr} from k_{rec} are shown in Table 4.

Table 4. Values for the rate constant for charge transfer k_{tr} from the interfacial states to the Al electrode along with a rate constant for interfacial recombination k_{rec} .

Non-Encapsulated (as-received)								
	k_{tr}				k_{rec}			
P3HT:PCBM	1:0.5	1:0.6	1:0.7	1:0.8	1:0.5	1:0.6	1:0.7	1:0.8
Photon Flux / cm² s⁻¹								
3.07·10¹⁶	1073	1521	1382	1923	1508	1060	1199	331
1.62·10¹⁷	3267	4058	3450	6339	4360	2602	3211	1288
2.95·10¹⁷	2298	5752	3683	7505	7702	2981	5051	2495

Non-Encapsulated (aged)								
	k_{tr}				k_{rec}			
P3HT:PCBM	1:0.5	1:0.6	1:0.7	1:0.8	1:0.5	1:0.6	1:0.7	1:0.8
Photon Flux / cm² s⁻¹								
3.07·10¹⁶	418	1290	1150	1415	2537	2094	1805	1166
1.62·10¹⁷	491	2846	2943	4228	8243	5887	5790	4505
2.95·10¹⁷	400	3452	2812	5835	11050	9659	8638	7276

However, the analysis of the results for case 2 shows a light intensity dependence not only for the recombination rate constant k_{rec} but also for the rate constant of the charge extraction k_{tr} , which does not have a clear physical meaning. The recombination rate constant could depend on the light intensity through the contribution of the majority carriers trapped in the P3HT phase, as discussed above; however, this should not affect the values of the charge transfer rate constant since majority carriers are not involved in charge extraction that occurs at the PCBM/Al interface. This model also cannot explain the variations of the parameters of IMPS plots on the PCBM content. Therefore, we must conclude that case 2 is not corroborated by the experimental data and therefore the photoprocess in our devices should be described by the mechanism outlined in case 1. Namely, the interfacial states where the charge recombination occurs are

1
2
3 located at the P3HT/PCBM and not the PCBM/Al interface; there is no charge extraction through
4 these interfacial states; all charge is extracted directly from PCBM at the PCBM/Al interface.
5
6

7
8 These conclusions have been recently corroborated by direct spatially resolved IMPS imaging of
9 P3HT/PCBM solar cells^{25,26} that showed high rates of recombination localized at the phase
10 boundaries between P3HT aggregates and PCBM crystallites. This also suggests that the origin
11 of the deep traps discussed in²⁴ is in fact related to interfacial states formed at the P3HT/PCBM
12 internal bulk heterojunction interface.
13
14
15
16
17
18
19
20
21
22
23

24 **Conclusions**

25
26
27 Bulk heterojunction organic solar cells containing varying amounts of PCBM were
28 investigated using steady-state J-V measurements in combination with the non-steady state
29 technique, intensity modulated photocurrent spectroscopy (IMPS). It was found that effective
30 encapsulation of the devices could prevent interfacial recombination from occurring. However,
31 for devices that were not encapsulated it was shown that interfacial recombination represents a
32 significant loss pathway for all PCBM contents. The enhanced recombination rate was attributed
33 to interfacial state formation due to reactions with atmospheric oxygen and moisture.
34
35
36
37
38
39
40
41
42
43
44

45 Two possible mechanisms were considered to identify the sites where interfacial
46 recombination was occurring. Detailed analysis of the IMPS data allowed us to determine that
47 interfacial recombination occurs at the internal P3HT/PCBM interface and that this process is
48 accelerated for lower PCBM contents because of less efficient extraction of photoexcited
49 carriers. Photoactive layers with the highest PCBM content showed the greatest stability with
50 time and exhibited reduced interfacial recombination. This fact highlights the stabilizing effect of
51
52
53
54
55
56
57
58
59
60

1
2
3 PCBM in organic solar cells that is sometimes overlooked when considering alternative acceptor
4 materials. At the same time, it also represents a possible limitation in the use of PCBM for
5 further improvements in device efficiency due to its high loading ratio, while contributing a
6 negligible amount towards light absorption and carrier generation. We also conclude that while
7 the interfacial states are responsible for interfacial recombination and the associated losses,
8 charge separation at the P3HT/PCBM bulk heterojunction does not involve those interfacial
9 states. This fact is also important because it shows that the best way to improve the device
10 efficiency is to suppress the formation of such interfacial states.
11
12
13
14
15
16
17
18
19
20
21
22

23 Our results highlight the utility in the use of IMPS for the characterization of various bulk
24 heterojunction systems. In particular, since IMPS spectra are sensitive to the presence of
25 interfacial states and can detect interfacial recombination, IMPS can be used as a powerful
26 diagnostic tool to predict the performance of organic solar cells. All devices in this study that
27 initially showed the presence of interfacial states as indicated by characteristic semicircle arcs in
28 the I quadrant of the IMPS spectra demonstrated deterioration of their performance due to
29 enhanced interfacial recombination, even without further exposure to atmospheric
30 contaminations. At the same time, none of the encapsulated devices showed any such arcs in the
31 IMPS spectra and their performance was stable with ageing.
32
33
34
35
36
37
38
39
40
41
42
43
44
45
46
47
48
49
50
51
52
53
54
55
56
57
58
59
60

1
2
3 AUTHOR INFORMATION
45
6 **Corresponding Author**
78
9 *E-mail: osemnik@uwo.ca
1011
12 Phone: +1 519 661 2111, ext. 82858.
1314
15 Fax: +1 519 661 3022
1617
18
19 **Present Addresses**
2021 [△] Present address. Department of Chemistry, University of Waterloo, 200 University Avenue
22
23 West, Waterloo, Ontario N2L 3G1, Canada
24
25
2627
28 **Author Contributions**
2930 The manuscript was written through contributions of all authors. All authors have given approval
31
32 to the final version of the manuscript.
33
3435
36 **ACKNOWLEDGMENT**
3738
39 O.A.S., J.C.B., and M.S. gratefully acknowledge the support by the Natural Sciences and
40
41 Engineering Research Council of Canada (NSERC), Strategic Partnership Program, project
42
43 STPGP 447326-13. O.A.S. and J.C.B. also acknowledge the support from NSERC Engage
44
45 Program, project EGP 396334 – 10. O.A.S. also acknowledges his NSERC Discovery Individual
46
47 grant. T.H. gratefully acknowledges the funding from CNRS and UNISTRA, Interreg IV Upper-
48
49 Rhine Valley Program, project C25. J.C.B. is also grateful for the graduate and postgraduate
50
51 scholarships from Ontario Graduate Scholarship Program (OGS) and Natural Sciences and
52
53 Engineering Research Council of Canada (NSERC PDF program).
54
55
56
57
58
59
60

REFERENCES

- (1) Byers, J. C.; Ballantyne, S.; Rodionov, K.; Mann, A.; Semenikhin, O. A. Mechanism of Recombination Losses in Bulk Heterojunction P3HT:PCBM Solar Cells Studied Using Intensity Modulated Photocurrent Spectroscopy. *ACS Appl. Mater. Interfaces* **2011**, *3*, 392–401.
- (2) Street, R. A.; Cowan, S.; Heeger, A. J. Experimental Test for Geminate Recombination Applied to Organic Solar Cells. *Phys. Rev. B* **2010**, *82*, 121301.
- (3) Street, R. A.; Schoendorf, M.; Roy, A.; Lee, J. H. Interface State Recombination in Organic Solar Cells. *Phys. Rev. B* **2010**, *81*, 205307.
- (4) Jørgensen, M.; Norrman, K.; Gevorgyan, S. A.; Tromholt, T.; Andreasen, B.; Krebs, F. C. Stability of Polymer Solar Cells. *Adv. Mater.* **2012**, *24*, 580–612.
- (5) Rösch, R.; Tanenbaum, D. M.; Jørgensen, M.; Seeland, M.; Bärenklau, M.; Hermenau, M.; Voroshazi, E.; Lloyd, M. T.; Galagan, Y.; Zimmermann, B.; Würfel, U.; Hösel, M.; Dam, H.F.; Gevorgyan, S.A.; Kudret, S.; Maes, W.; Lutsen, L.; Vanderzande, D.; Andriessen, R.; Teran-Escobar, G.; Lira-Cantu, M.; Rivaton, A.; Uzunoğlu, G.Y.; Germack, D.; Andreasen, B.; Madsen, M.V.; Norrman, K.; Hoppe, H.; Krebs, F.C. Investigation of the Degradation Mechanisms of a Variety of Organic Photovoltaic Devices by Combination of Imaging Techniques—the ISOS-3 Inter-Laboratory Collaboration. *Energy Environ. Sci.* **2012**, *5*, 6521-6540.
- (6) Teran-Escobar, G.; Tanenbaum, D. M.; Voroshazi, E.; Hermenau, M.; Norrman, K.; Lloyd, M. T.; Galagan, Y.; Zimmermann, B.; Hösel, M.; Dam, H. F.; Jørgensen, M.; Gevorgyan, S.; Kudret, S.; Maes, W.; Lutsen, L.; Vanderzande, D.; Würfel, U.; Andriessen, R.; Rösch, R.; Hoppe, H.; Rivaton, A.; Uzunoğlu, G. Y.; Germack, D.;

- 1
2
3
4
5
6
7
8
9
10
11
12
13
14
15
16
17
18
19
20
21
22
23
24
25
26
27
28
29
30
31
32
33
34
35
36
37
38
39
40
41
42
43
44
45
46
47
48
49
50
51
52
53
54
55
56
57
58
59
60
- Andreasen, B.; Madsen, M. V.; Bundgaard, E.; Krebs, F. C.; Lira-Cantu, M. On the Stability of a Variety of Organic Photovoltaic Devices by IPCE and in Situ IPCE Analyses--the ISOS-3 Inter-Laboratory Collaboration. *Phys. Chem. Chem. Phys.* **2012**, *14*, 11824–11845.
- (7) Norrman, K.; Krebs, F. C. Lifetimes of Organic Photovoltaics: Using TOF-SIMS and ¹⁸O Isotopic Labelling to Characterise Chemical Degradation Mechanisms. *Sol. Energy Mater. Sol. Cells* **2006**, *90*, 213–227.
- (8) Norrman, K.; Larsen, N. B.; Krebs, F. C. Lifetimes of Organic Photovoltaics: Combining Chemical and Physical Characterisation Techniques to Study Degradation Mechanisms. *Sol. Energy Mater. Sol. Cells* **2006**, *90*, 2793–2814.
- (9) Norrman, K.; Gevorgyan, S. A.; Krebs, F. C. Water-Induced Degradation of Polymer Solar Cells Studied by H₂(¹⁸O) Labeling. *ACS Appl. Mater. Interfaces* **2009**, *1*, 102–112.
- (10) Jørgensen, M.; Norrman, K.; Krebs, F. C. Stability/degradation of Polymer Solar Cells. *Sol. Energy Mater. Sol. Cells* **2008**, *92*, 686–714.
- (11) Krebs, F. C.; Norrman, K. Analysis of the Failure Mechanism for a Stable Organic Photovoltaic during 10 000 H of Testing. *Prog. Photovoltaics* **2007**, *15*, 697–712.
- (12) Petersen, M. H.; Gevorgyan, S. A.; Krebs, F. C. Thermocleavable Low Band Gap Polymers and Solar Cells Therefrom with Remarkable Stability toward Oxygen. *Macromolecules* **2008**, *41*, 8986–8994.
- (13) Zimmermann, B.; Würfel, U.; Niggemann, M. Longterm Stability of Efficient Inverted P3HT:PCBM Solar Cells. *Sol. Energy Mater. Sol. Cells* **2009**, *93*, 491–496.
- (14) Steim, R.; Kogler, F. R.; Brabec, C. J. Interface Materials for Organic Solar Cells. *J. Mater. Chem.* **2010**, *20*, 2499.

- 1
2
3
4
5
6
7
8
9
10
11
12
13
14
15
16
17
18
19
20
21
22
23
24
25
26
27
28
29
30
31
32
33
34
35
36
37
38
39
40
41
42
43
44
45
46
47
48
49
50
51
52
53
54
55
56
57
58
59
60
- (15) Krebs, F. C. Encapsulation of Polymer Photovoltaic Prototypes. *Sol. Energy Mater. Sol. Cells* **2006**, *90*, 3633–3643.
- (16) Seemann, A.; Sauermann, T.; Lungenschmied, C.; Armbruster, O.; Bauer, S.; Egelhaaf, H.-J.; Hauch, J. Reversible and Irreversible Degradation of Organic Solar Cell Performance by Oxygen. *Sol. Energy* **2011**, *85*, 1238–1249.
- (17) Schafferhans, J.; Baumann, A.; Wagenpfahl, A.; Deibel, C.; Dyakonov, V. Oxygen Doping of P3HT:PCBM Blends: Influence on Trap States, Charge Carrier Mobility and Solar Cell Performance. *Org. Electron.* **2010**, *11*, 1693–1700.
- (18) Manceau, M.; Rivaton, A.; Gardette, J.-L.; Guillerez, S.; Lemaître, N. Light-Induced Degradation of the P3HT-Based Solar Cells Active Layer. *Sol. Energy Mater. Sol. Cells* **2011**, *95*, 1315–1325.
- (19) Kumar, M.; Dubey, A.; Reza, K. M.; Adhikari, N.; Qiao, Q.; BommiSETTY, V. Origin of Photogenerated Carrier Recombination at the Metal-Active Layer Interface in Polymer Solar Cells. *Phys. Chem. Chem. Phys.* **2015**, *17*, 27690–27697.
- (20) MacKenzie, R. C. I.; Balderrama, V. S.; Schmeisser, S.; Stoof, R.; Greedy, S.; Pallarès, J.; Marsal, L. F.; Chanaewa, A.; von Hauff, E. Loss Mechanisms in High Efficiency Polymer Solar Cells. *Adv. Energy Mater.* **2016**, *6*, 1501742.
- (21) Shao, G.; Glaz, M. S.; Ma, F.; Ju, H.; Ginger, D. S. Intensity-Modulated Scanning Kelvin Probe Microscopy for Probing Recombination in Organic Photovoltaics. *ACS Nano* **2014**, *8*, 10799–10807.
- (22) Set, Y. T.; Li, B.; Lim, F. J.; Birgersson, E.; Luther, J. Analytical Modeling of Intensity-Modulated Photovoltage Spectroscopic Responses of Organic Bulk-Heterojunction Solar Cells. *Appl. Phys. Lett.* **2015**, *107*, 173301.

- 1
2
3
4
5
6
7
8
9
10
11
12
13
14
15
16
17
18
19
20
21
22
23
24
25
26
27
28
29
30
31
32
33
34
35
36
37
38
39
40
41
42
43
44
45
46
47
48
49
50
51
52
53
54
55
56
57
58
59
60
- (23) Pockett, A.; Eperon, G. E.; Peltola, T.; Snaith, H. J.; Walker, A.; Peter, L. M.; Cameron, P. J. Characterization of Planar Lead Halide Perovskite Solar Cells by Impedance Spectroscopy, Open-Circuit Photovoltage Decay, and Intensity-Modulated Photovoltage/Photocurrent Spectroscopy. *J. Phys. Chem. C* **2015**, *119*, 3456–3465.
- (24) Set, Y. T.; Heinemann, M. D.; Birgersson, E.; Luther, J. On the Origin of the Quadrant I Semicircle in Intensity-Modulated Photocurrent Spectra of P3HT:PCBM Bulk Heterojunction Solar Cells: Evidence of Degradation-Related Trap-Assisted Recombination. *J. Phys. Chem. C* **2013**, *117*, 7993–8000.
- (25) Gao, J.; Thomas, A. K.; Johnson, R.; Guo, H.; Grey, J. K. Spatially Resolving Ordered and Disordered Conformers and Photocurrent Generation in Intercalated Conjugated Polymer/Fullerene Blend Solar Cells. *Chem. Mater.* **2014**, *26*, 4395–4404.
- (26) Gao, Y.; Wise, A. J.; Thomas, A. K.; Grey, J. K. Spectroscopic and Intensity Modulated Photocurrent Imaging of Polymer/Fullerene Solar Cells. *ACS Appl. Mater. Interfaces* **2016**, *8*, 285–293.
- (27) Jouane, Y.; Colis, S.; Schmerber, G.; Kern, P.; Dinia, A.; Heiser, T.; Chapuis, Y.-A. Room Temperature ZnO Growth by Rf Magnetron Sputtering on Top of Photoactive P3HT: PCBM for Organic Solar Cells. *J. Mater. Chem.* **2011**, *21*, 1953.
- (28) Chirvase, D.; Parisi, J.; Hummelen, J. C.; Dyakonov, V. Influence of Nanomorphology on the Photovoltaic Action of Polymer–fullerene Composites. *Nanotechnology* **2004**, *15*, 1317–1323.
- (29) Li, J.; Peter, L. M. Surface Recombination at Semiconductor Electrodes. Part III. Steady-state and intensity modulated photocurrent response. *J. Electroanal. Chem.* **1985**, *193*, 27–47.

- 1
2
3
4
5
6
7
8
9
10
11
12
13
14
15
16
17
18
19
20
21
22
23
24
25
26
27
28
29
30
31
32
33
34
35
36
37
38
39
40
41
42
43
44
45
46
47
48
49
50
51
52
53
54
55
56
57
58
59
60
- (30) Li, J.; Peter, L. M. Surface Recombination at Semiconductor Electrodes. Part IV. Steady-state and intensity modulated photocurrents at n-GaAs electrodes. *J. Electroanal. Chem.* **1986**, *199*, 1–26.
- (31) Peter, L. M. Dynamic Aspects of Semiconductor Photoelectrochemistry. *Chem. Rev.* **1990**, *90*, 753–769.
- (32) Rotenberg, Z. A.; Semenikhin, O. A. Intensity Modulated Photocurrents on an Anodically Oxidized Lead Electrode in Sulfuric Acid Solution. *J. Electroanal. Chem.* **1991**, *316*, 165–174.
- (33) Semenikhin, O. A.; Kazarinov, V. E.; Jiang, L.; Hashimoto, K.; Fujishima, A. Suppression of Surface Recombination on TiO₂ Anatase Photocatalysts in Aqueous Solutions Containing Alcohol. *Langmuir* **1999**, *15*, 3731–3737.
- (34) DiCarmine, P. M.; Semenikhin, O. A. Intensity Modulated Photocurrent Spectroscopy (IMPS) of Solid-State Polybithiophene-Based Solar Cells. *Electrochim. Acta* **2008**, *53*, 3744–3754.
- (35) Tremolet de Villers, B.; Tassone, C. J.; Tolbert, S. H.; Schwartz, B. J. Improving the Reproducibility of P3HT:PCBM Solar Cells by Controlling the PCBM/Cathode Interface. *J. Phys. Chem. C* **2009**, *113*, 18978–18982.
- (36) Peter, L. M.; Wijayantha, K. G. U.; Tahir, A. A. Kinetics of Light-Driven Oxygen Evolution at α -Fe₂O₃ Electrodes. *Faraday Discuss.* **2012**, *155*, 309.

